

Toward a Framework for Incorporating MJO and ENSO Information into CPC Probabilistic Extended Range Forecasts

Nat Johnson¹, Emily Riddle², Marshall Stoner³,
Steven Feldstein⁴, Dan Collins³, Michelle L'Heureux³

¹*IPRC, University of Hawaii at Manoa*

²*Wyle Information Systems, Climate Prediction Center, NCEP/NWS/NOAA*

³*Climate Prediction Center, NCEP/NWS/NOAA*

⁴*Pennsylvania State University*

1. Introduction

Numerous studies have discussed the role of the El Niño/Southern Oscillation (ENSO) in providing a source of skill in climate prediction on seasonal timescales across much of the globe, particularly over the Pacific/North America region. More recently, studies have shown that the dominant form of variability in the tropics on intraseasonal timescales, the Madden-Julian Oscillation (MJO), also impacts patterns of intraseasonal variability in the northern hemisphere extratropics, providing a possible source of predictive skill over this region on intraseasonal timescales. By modulating tropical convection, the MJO can initiate poleward propagating Rossby waves that impact extratropical weather patterns and influence the leading patterns of low-frequency northern hemisphere variability, the Arctic Oscillation (AO) and Pacific North America pattern (PNA) (*e.g.*, Higgins and Mo 1997, L'Heureux and Higgin 2008, Cassou 2008, Mori and Watanabe 2008, Lin *et al.* 2009, Johnson and Feldstein 2010). Through these mechanisms, the MJO may provide some degree of enhanced predictability for precipitation and temperature in the northern hemisphere extratropics, especially during the winter months at extended range timescales (~10 – 30 days) (*e.g.*, Cassou 2008, Vitart and Molteni 2010, Lin and Brunet 2010, Jones *et al.* 2011).

One challenge for forecasters at NOAA Climate Prediction Center (CPC) is finding a way to incorporate these known relationships among the MJO, ENSO, and the large-scale atmospheric circulation into existing extended-range forecast products for the one-to-four week time period. In an effort to provide a framework for incorporating these influences, we present preliminary results that demonstrate a strong influence of the MJO and ENSO on the frequency of winter geopotential height patterns over the PNA region. The purpose of this study is 1) to explore when and for how long tropical MJO activity impacts commonly occurring intraseasonal climate patterns over North America and the surrounding oceans; and 2) to examine how these impacts change during different phases of ENSO. In addition, we discuss the potential for a Bayesian framework to combine this information with dynamical model forecast performance to generate enhanced extended-range forecasts in the one-to-four week time period.

2. Data and methods

We characterize the continuum of wintertime 500 hPa geopotential height patterns in the PNA region with the use of k-means cluster analysis (*e.g.*, Michelangeli *et al.* 1995, Johnson and Feldstein 2010). The method of k-means clustering essentially partitions a potentially large, high-dimensional dataset to a smaller number (K) of representative clusters. Each seven-day geopotential height field (described below) is assigned to a best-matching cluster, and each cluster centroid represents the mean of all height fields assigned to the cluster. Because the method essentially maximizes the similarity between the seven-day height fields and their corresponding cluster centroids, we have reasonable assurance that the resulting centroids correspond with physical, representative patterns.

The cluster analysis is performed on 500 hPa height anomalies from the NCEP/NCAR reanalysis at 2.5° x 2.5° resolution. Only days during the winter months (DJFM) are considered over years ranging from January

1979 to March 2011. This time period is chosen to match the dates when outgoing longwave radiation (OLR) data are also available to compute the MJO index (discussed below). The domain for the cluster analysis ranges from 20°N to 87.5°N and from 157.5°E to 2.5°W, covering North America and the surrounding ocean basins. This domain was chosen because it encompasses regions with the strongest MJO response, and because our focus is on prediction over North America. Anomalies in the 500-hPa height data are calculated with respect to the daily 1981-2010 climatology, and smoothed by a flat seven-day filter. The cluster analysis is performed on the smoothed daily height anomalies. This smoothing ensures that the cluster analysis focuses on large scale features in the height field and matches the averaging timescale of extended range week-2, week-3 and week-4 forecasts.

To examine how the MJO affects the cluster occurrence frequencies, we must identify periods when the MJO is active, and summarize the spatial location and propagation of MJO during these periods. To do this, we use the Wheeler-Hendon MJO index (Wheeler and Hendon 2004) as provided by the Australian Bureau of Meteorology. The index is derived from the leading two empirical orthogonal functions (EOFs) of three combined fields: tropical OLR, equatorial zonal wind at 850 hPa, and equatorial zonal wind at 200 hPa. Based on the values of these leading EOFs, the Wheeler-Hendon (WH) index traces through eight phases as the MJO signature propagates eastward. Between phase 2 and phase 6, for example, a convectively active region propagates from the western Indian Ocean across the maritime continent and into the western Pacific. The OLR and zonal wind signatures of each phase of the MJO are referenced in a number of previous papers (*e.g.*, Wheeler and Hendon 2004, Cassou *et al.* 2008, Johnson and Feldstein 2010) and can be viewed on the CPC website, <http://www.cpc.ncep.noaa.gov/products/precip/CWlink/MJO/Composites/Tropical/>.

Following L'Heureux and Higgins (2008) we identify active MJO events based on a pentad-averaged version of the WH index. An MJO episode is identified when the following requirements are met for at least six consecutive pentads: 1) The index amplitude is greater than one and 2) The index phase progresses in a counter-clockwise direction without reversing directions or stalling in a particular phase for more than four pentads. El Niño, La Niña and neutral days are classified by month based on the central month in the Oceanic Niño Index (ONI) definition provided on the CPC website.

3. Results

3.1 Geopotential height cluster patterns

In Figure 1 we show the seven 500 hPa geopotential height cluster patterns that represent the continuum of dominant wintertime teleconnection patterns in the Pacific/North America region. The choice of seven for K is based on an optimal volume index ratio, which essentially signifies the number of cluster patterns that efficiently cover the hyperspace without excessive cluster overlap, as described more thoroughly in Riddle *et al.* (2011). Overall, the results we present, however, are not sensitive to the precise choice of K . The seven cluster patterns bear a strong resemblance to well known teleconnection patterns such as the positive (clusters

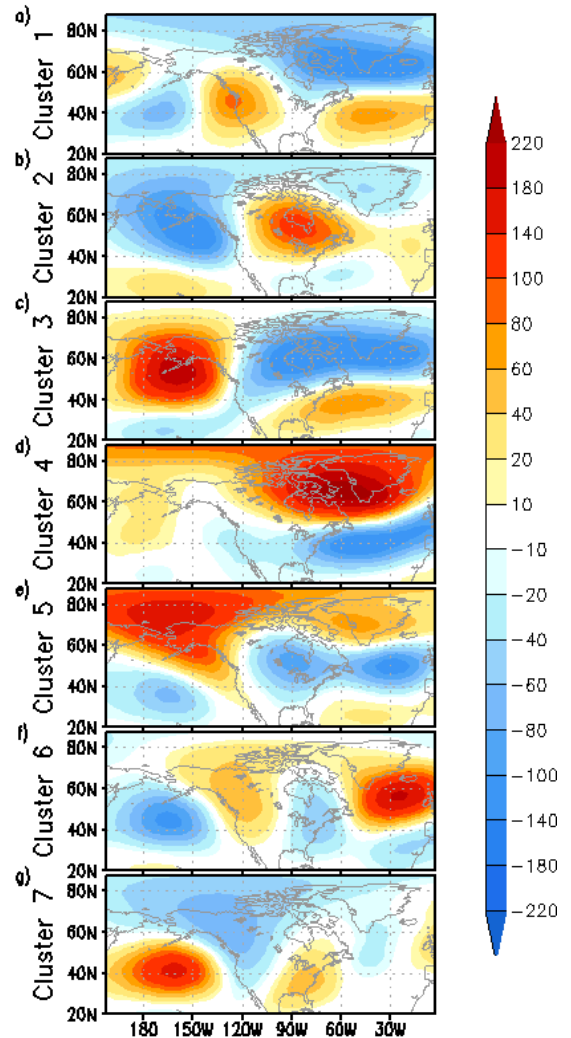


Fig. 1 K-means cluster centroid patterns of 500 hPa geopotential height anomalies (m) over the extended North America region.

2 and 6) and negative (clusters 3 and 7) phases of the PNA as well as the positive (clusters 1 and 3) and negative (clusters 4 and 6) phases of the North Atlantic Oscillation (NAO)/AO.

The remainder of this paper focuses on clusters 4, 6 and 7 because, unlike the other four clusters, these three clusters are significantly influenced by MJO activity, as discussed in the next section. Clusters 4, 6, and 7 are associated with substantial upper tropospheric zonal wind, precipitation, and surface temperature anomalies over regions of the continental United States (Figure 2). In particular, the negative phase AO-like cluster 4 is associated with a southward shift of the North American jet exit region, and a merging of this jet with the entrance region of the North African jet (Fig. 2a). In association with this southward shift, cluster 4 features widespread cold anomalies across the eastern and mid-western United States (Fig. 2g) and a southward shift in the storm track that is reflected in the precipitation anomalies (Fig. 2d).

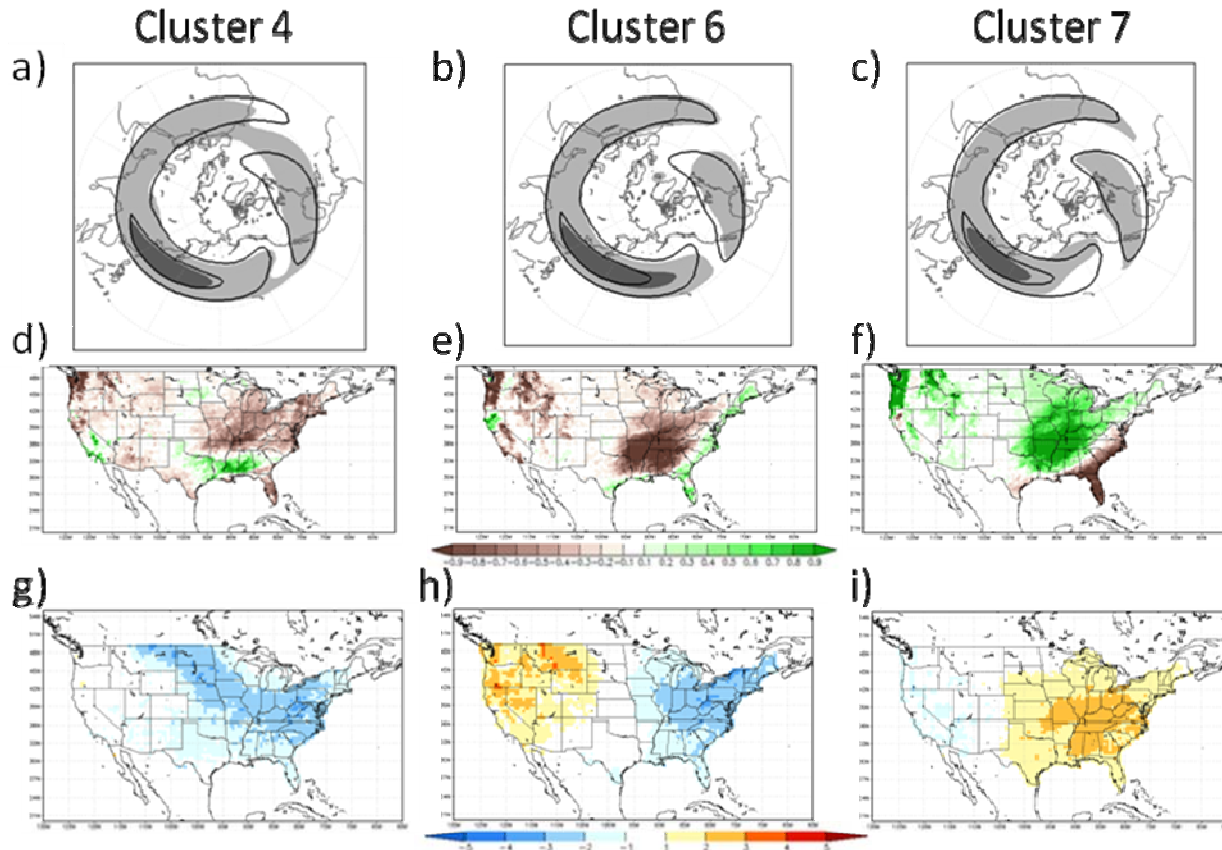


Fig 2 (a) – (c) Shading shows 25 m/s (light grey) and 50 m/s (dark grey) contours for a composite of 200 hPa zonal winds for all days in Clusters 4, 6, and 7 compared with the same two contours for the winter (DJFM) climatology (solid lines). (d) – (i) Composite of (d,e,f) precipitation and (g,h,i) temperature anomalies over the United States for all winter days in Clusters 4, 6, and 7. Zonal wind data are from the NCEP reanalysis, surface temperature composites are derived from the gridded daily cooperative dataset of Janowiak *et al.* (1999), and the precipitation composites are derived from the Climate Prediction Center Merged Analysis of Precipitation (CMAP) (Xie and Arkin 1997).

Over the Pacific, the positive phase PNA-like cluster 6 is associated with a strengthening and southward shift of the jet exit region of the East Asian jet (Fig. 2b). Although both cluster 6 and 4 are associated with negative AO index values, the two clusters have very different signatures in terms of perturbations to jets over the North Atlantic. Cluster 4 is associated with an extension and southward shift of the jet exit region in the Atlantic whereas cluster 6 is associated mainly with a retraction of the North American jet over the Atlantic. Rainfall anomalies over the continental United States for cluster 6 are positive along the eastern coastal US and negative over an extensive region in the interior southeastern states and the Midwest (Fig. 2e). Except for

a wet region in northern California, dry anomalies are also observed over most of the west coast and western mountain states. Temperature anomaly composites are negative over the eastern US and positive over the western and northern mountain states in association with the PNA ridge-trough pattern (Fig. 2h).

The negative phase PNA-like cluster 7 composites (Fig. 2c, f, i) largely oppose those of cluster 6. The biggest asymmetry is seen in the temperature composites: whereas cluster 6 is associated with widespread warm anomalies over the western states (Fig. 2h), cluster 7 features only weak anomalies in the west (Fig. 2i).

3.2 Influence of ENSO and the MJO on cluster pattern frequency of occurrence

To examine how the frequency of cluster occurrence is modulated in the days and weeks following an MJO event and during different phases of ENSO, we follow a very similar approach to that of Cassou (2008). Like Cassou, we examine how the frequency of a cluster occurring under certain external conditions E (e.g., 7 days after the MJO is active in phase 1) is elevated or suppressed with respect to the cluster's climatological frequency of occurrence over all 3962 days. The percent change in frequency, C , is a function of the external conditions, E , and the cluster number i :

$$C(i, E) = 100 * \left[\frac{\left(\frac{N_{i,E}}{N_E} - \frac{N_i}{N_T} \right)}{\frac{N_i}{N_T}} \right] \quad (1)$$

where N_T is 3962, the total number of days in the study, N_i is the number of times in the study that cluster i occurs, N_E is the number of days when the external conditions, E , are met, and $N_{i,E}$ is the number of times that cluster i occurs under the conditions E . The percentage $C(i, E)$ is equal to 100 if cluster i occurs twice as frequently under the conditions E as it does in the full record, and is equal to -100 if the cluster never occurs under the conditions E . C is calculated for a range of external conditions, E , including an active MJO during each of the 8 phases and at lead times ranging from zero to 40 days, and for La Niña and El Niño MJO days only. In all of these cases, the full reference climatology is always used for comparison.

Figure 3 shows C as a function of lag with respect to MJO phase for clusters 4, 6, and 7. For each cluster pattern in Fig. 3, we consider all MJO episodes and MJO episodes during El Niño and La Niña episodes only. Statistical significance of C is assessed with a Monte Carlo test whereby 10,000 synthetic, first-order Markov chain cluster pattern time series are generated with transition probabilities that follow the observed transition probabilities, as discussed more thoroughly in Riddle et al. (2011). Moreover, global significance, which tests against the null hypothesis that the MJO has no overall effect on cluster frequency of occurrence, is assessed by controlling the “false discovery rate” (Benjamini and Hochberg 1995, Wilks 2006). Again, further details can be found in Riddle et al. (2011).

Consistent with previous studies, Figure 3 reveals that the MJO exerts a significant influence on the dominant teleconnection patterns of the Pacific/North America region over lags of a few weeks. The occurrence frequency of cluster 4, which resembles a negative AO, is elevated significantly with respect to climatology following active MJO episodes in phases 6 and 7 (Fig. 3a), which are indicative of enhanced convection and upper level divergence over the eastern Pacific Ocean, and suppressed convection and upper level convergence over the western Pacific and maritime continent. The largest positive anomalies in these frequencies occur approximately 20-25 days after MJO phase 6, and approximately 8-13 days after phase 7. Under these conditions Cluster 4 occurs between 2 and 2.5 times as likely as it is in the overall climatology. Though weaker, significant anomalies are observed as far out as 40 days after an occurrence of MJO phase 5. The most significant suppression of Cluster 4 frequencies occurs approximately 24-28 days after phase 2 of the MJO and 18-22 days after phase 3 of the MJO. The phasing of these responses is expected and consistent with an MJO signal propagating from phase 1 through phase 8. The results shown in Figure 3a are consistent with findings from L'Heureux and Higgins (2008), Cassou (2008), Roundy et al. (2010), and others who have noted an increase in negative AO events approximately 10-20 days after the occurrence of an MJO phase 6-7 event. Moreover, Fig. 3a shows that this enhancement is more pronounced during El Niño episodes relative

to La Niña episodes, which is consistent with findings that ENSO can modulate the response to the MJO (Schrage *et al.* 1999, Roundy *et al.* 2010, Moon *et al.* 2011).

Figure 3b shows that the frequencies of cluster 6 are elevated significantly with respect to climatology following active MJO episodes in phases 5 and 6, which are indicative of convection and upper level divergence over the central Pacific, and suppressed convection and upper level convergence over the maritime continent and eastern Indian Ocean. The strongest positive anomalies occur 23-26 days after MJO phase 5, and 12-14 days after MJO phase 6. These results are consistent with previous studies that link an increase in

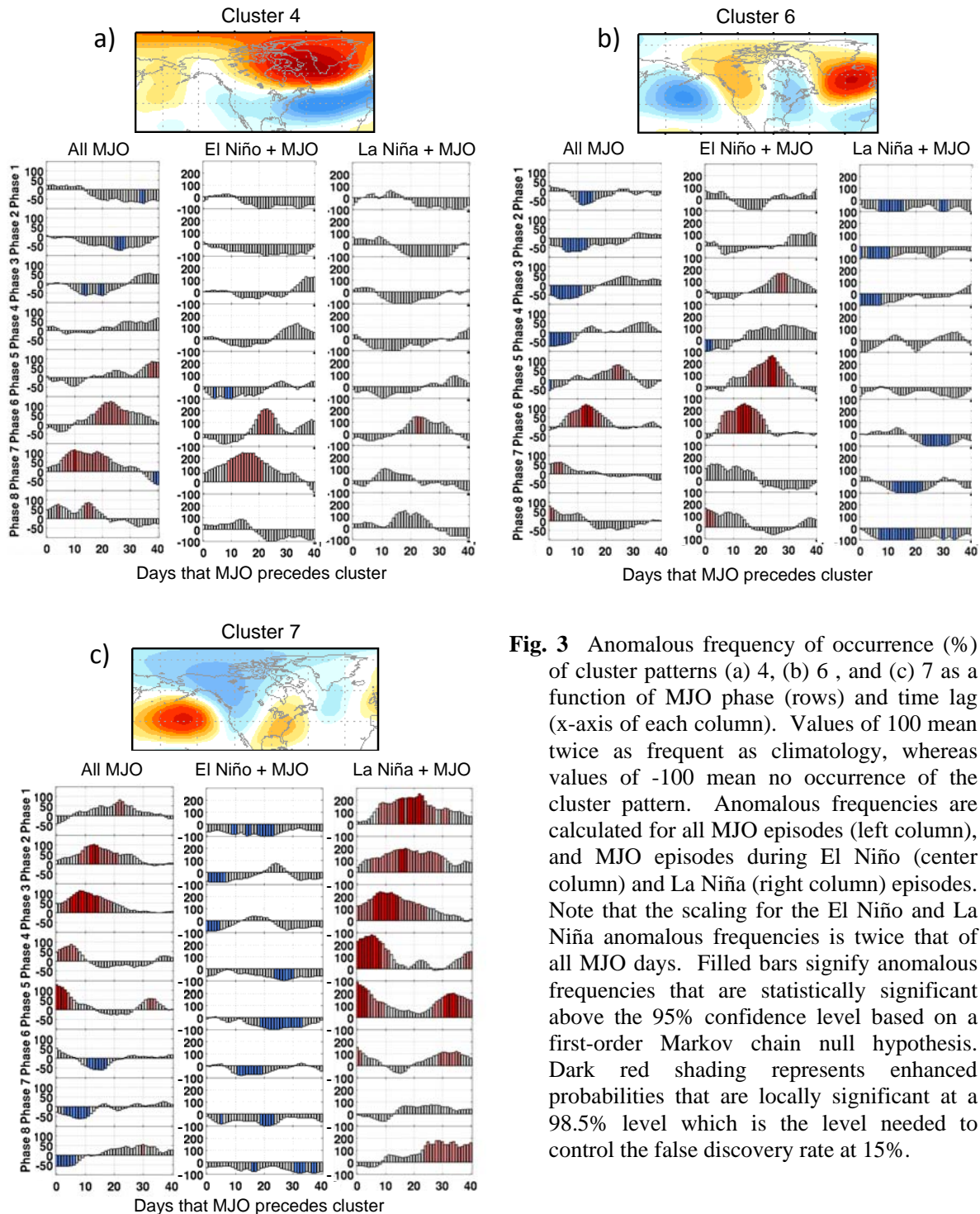


Fig. 3 Anomalous frequency of occurrence (%) of cluster patterns (a) 4, (b) 6, and (c) 7 as a function of MJO phase (rows) and time lag (x-axis of each column). Values of 100 mean twice as frequent as climatology, whereas values of -100 mean no occurrence of the cluster pattern. Anomalous frequencies are calculated for all MJO episodes (left column), and MJO episodes during El Niño (center column) and La Niña (right column) episodes. Note that the scaling for the El Niño and La Niña anomalous frequencies is twice that of all MJO days. Filled bars signify anomalous frequencies that are statistically significant above the 95% confidence level based on a first-order Markov chain null hypothesis. Dark red shading represents enhanced probabilities that are locally significant at a 98.5% level which is the level needed to control the false discovery rate at 15%.

convection over the central Pacific with a strengthening of the local Hadley circulation, an extension of the East Asian jet over the Pacific, and the development of a cyclonic circulation anomaly over the northern Pacific. Higgins and Mo (1997) and Hoskins and Karoly (1981) and others show that positive anomalies in the PNA occur approximately 10 days following MJO phase 6, in line with the results presented here. Consistent with this finding, the anomalous frequencies of the negative PNA-like cluster 7 (Fig. 3c) are generally opposite to those of cluster 6. The strongest changes in frequency occur simultaneously with MJO phase 5, 3-8 days after phase 4, 8-12 days after phase 3, and 12-16 days after phase 2. These are consistent with studies that suggest that negative PNA anomalies occur approximately 10 days after phase 3, which is indicative of suppressed convection and upper level convergence over the central Pacific. Figures 3b and c reveal that the response of clusters 6 and 7 to the MJO is substantially altered by ENSO. In fact, the enhanced probabilities of cluster 6 (cluster 7) following phase 6 (phase 2) of the MJO are completely absent in La Niña (El Niño) years. This may be expected given that convection anomalies over the Pacific are in phase between El Niño (La Niña) and phase 6 (phase 2) of the MJO.

4. Future work

The preceding analysis demonstrates that the MJO significantly impacts atmospheric circulation patterns with strong surface temperature and precipitation signatures in the continental United States for lead times generally between one and four weeks. An important question remains: how can forecasters at NOAA CPC use this information to enhance extended range forecasts? A suitable framework should incorporate both the expected MJO impacts and the information provided by dynamical model forecast guidance. We propose to merge these two sources of information in a framework based on Bayes' theorem. In the present context, we informally may express Bayes' theorem by

$$P(\theta_j|f_j) \propto P(\theta_j)P(f_j|\theta_j), \quad (2)$$

where $P(\theta_j|f_j)$ is the probability of the occurrence of cluster pattern j , given the model forecast of cluster pattern j in the time period of interest. Bayes' theorem states that the posterior probability, $P(\theta_j|f_j)$, which reflects the forecaster's confidence in the occurrence of cluster j , is proportional to the prior probability $P(\theta_j)$ multiplied by the conditional probability $P(f_j|\theta_j)$. In our proposed application, the expected, combined influence of the MJO and ENSO provides the forecaster with prior information (*i.e.*, before viewing the patterns forecast by the dynamical models) on the occurrence of each cluster pattern that can be incorporated into $P(\theta_j)$. In addition, archived model hindcasts may provide information on model forecast performance that can be used to construct $P(f_j|\theta_j)$. Therefore, Bayes' theorem provides a basic framework with which both the expected MJO/ENSO influence can be combined with dynamical model forecast performance to generate probabilities of cluster pattern occurrence in the forecast period of interest. These posterior probabilities then may be used to weight model forecast fields in a multi-model ensemble forecast. Current efforts are focused on converting this informal framework into a formal Bayesian forecast system for extended range forecasts in the one- to four-week time period.

References

- Benjamini, Y., and Y. Hochberg, 1995: Controlling the false discovery rate: A practical and powerful approach to multiple testing. *J. Roy. Statist. Soc. Ser. B (Methodological)*, **57**, 289-300.
- Cassou, C., 2008: Intraseasonal interaction between the Madden-Julian Oscillation and the North Atlantic Oscillation. *Nature*, **455**, 523-527.
- Higgins, R. W., and K. C. Mo, 1997: Persistent North Pacific circulation anomalies and the tropical intraseasonal oscillation. *J. Climate*, **10**, 223-244.
- Hoskins, B.J., and D. J. Karoly, 1981: The steady linear response of a spherical atmosphere to thermal and orographic forcing. *J. Atmos. Sci.*, **38**, 1179-1196.
- Janowiak, J. E., G. D. Bell, and M. Chelliah. 1999: *A gridded data base of daily temperature maxima and minima for the conterminous United States: 1948-1993*. U.S. Department of Commerce, National Oceanic and Atmospheric Administration, National Weather Service (Washington, D.C.), 49 pp.

- Johnson, N. C, and S. B. Feldstein. 2010. The continuum of North Pacific sea level pressure patterns: Intraseasonal, interannual, and interdecadal variability. *J. Climate*, **23**, 851-867.
- Jones, C., J. Gottschalck, L. M. V. Carvalho, and W. Higgins, 2011: Influence of the Madden-Julian Oscillation on forecasts of extreme precipitation in the contiguous United States. *Mon. Wea. Rev.*, **139**, 332-350.
- L'Heureux, M. L., and R. W. Higgins, 2008: Boreal winter links between the Madden-Julian Oscillation and the Arctic oscillation. *J. Climate*, **21**, 3040-3050.
- Lin, H., G Brunet, and J. Derome, 2009: An observed connection between the North Atlantic Oscillation and the Madden-Julian Oscillation. *J. Climate*, **22**, 364-380.
- Lin, H., and G. Brunet, 2010: The influence of the Madden-Julian Oscillation on Canadian wintertime surface air temperature. *Mon. Wea. Rev.*, **137**, 2250-2262.
- Michelangeli, P.- A, R. Vautard, and B. Legras, 1995: Weather regimes: Recurrence and quasi stationarity. *J. Atmos. Sci.*, **52**, 1237-1256.
- Moon, J-Y., B. Wang, and K-J. Ha, 2011. ENSO regulation of MJO teleconnection. *Climate Dyn.*, **37**, 1133-1149.
- Mori, M., and M. Watanabe, 2008: The growth and triggering mechanisms of the PNA: A MJO-PNA coherence. *J. Meteor. Soc. Japan*, **86**, 213-236.
- Riddle, E., M. Stoner, D. Collins, S. Feldstein, N. C. Johnson, and M. L'Heureux, 2011: The impact of ENSO and the MJO on wintertime intraseasonal climate patterns over the Pacific/North America region. To be submitted to *J. Climate*.
- Roundy, P. E., K. MacRitchie, J. Asuma, and T. Melino, 2010: Modulation of the global atmospheric circulation by combined activity in the Madden-Julian Oscillation and the El Niño-Southern Oscillation during boreal winter. *J. Climate*, **23**, 4045-4059.
- Schrage, J. M, D. G. Vincent, and A. H. Fink, 1999: Modulation of intraseasonal (25-70 day) processes by the superimposed ENSO cycle across the Pacific basin. *Meteor. Atmos. Phys.*, **70**, 15-27.
- Vitart, F., and F. Molteni, 2010: Simulation of the Madden-Julian Oscillation and its teleconnections in the ECMWF forecast system. *Quart. J. Roy. Meteor. Soc.*, **136**, 842-855.
- Wilks, D. S., 2006: On 'field significance' and the false discovery rate. *J. Appl. Meteor. Climatol.*, **45**, 1181-1189.
- Wheeler, M. C., and H. H. Hendon, 2004: An all-season real-time multivariate MJO index: Development of an index for monitoring and prediction. *Mon. Wea. Rev.*, **132**, 1917-1932.
- Xie, P., and P. A Arkin, 1997: Global precipitation: A 17-year monthly analysis based on gauge observations, satellite estimates, and numerical model outputs. *Bull. Amer. Meteor. Soc.*, **78**, 2539-2558.